Molecular Model for the Mechanical Properties of Elastomers. 1. Network Formation and Role of Entanglements

Yves Termonia

Central Research and Development, Experimental Station, E.I. du Pont de Nemours, Inc., Wilmington, Delaware 19898. *Received December 9, 1988; Revised Manuscript Received March 6, 1989*

ABSTRACT: A molecular model has been developed for the study of the factors controlling the deformation behavior of cross-linked elastomers. The model allows a detailed analysis of both the network connectivity upon cross-linking and of the mechanical properties upon tensile deformation. In contrast to previous work, entanglements latent in the polymer prior to cross-linking are explicitly taken into account. Chain slippage is also allowed for through a detailed analysis of the force gradients near entanglement points. The model has been applied to elastomeric networks formed through end linking of difunctional polymer chains with plurifunctional junction sites. The dependence of mechanical properties on molecular weight of the starting polymer, cross-link functionality, and degree of advancement of the reaction are studied. The results show that entanglements are expected to dominate the deformation behavior of most commercial cross-linked elastomers. Furthermore, the empirical Mooney–Rivlin relation between modulus and draw ratio is recovered and fully explained in terms of chain slippage through entanglements.

1. Introduction

A theoretical description of the factors controlling the performance properties of elastomers faces two major challenges. The first is to devise a realistic model for network formation during cross-linking. Previous network models can be divided into two categories:[1] (a) Flory–Stockmayer types of approaches, which neglect cyclic bonds and exclude volume effects,[2,3] and (b) computer simulations in space, which allow the formation of rings of any size.[4,5]

The second problem is to relate the elastic properties of those networks to their molecular structure. There is at present no firm molecular model for describing the role of entanglements on the stress–strain behavior of elastomeric systems. Previous approaches were only phenomenological or semiempirical and have led to two opposing views. Earlier studies by Flory[6] and Ronca[7] limit the role of chain–chain interactions to that of restricting fluctuations in network junctions. A more concise treatment of these constraining effects can be found in ref 8. At small strains, all junction fluctuations are suppressed and the shear modulus, defined through

$$G = \nu kT \tag{1}$$

takes on its "chemical" value for which ν equals the number of *starting chains* per unit volume.[6-8] The above point of view has been challenged by many other researchers[9-14] who contend that chain–chain interactions are also present along the chain contour and add a significant contribution to the modulus value given by eq 1. Entanglements along chain contours have been modeled as confining tubes,[15,16] hoops,[17] or slipping links.[18]

The object of the present work is to introduce a new model for the mechanical properties of elastomeric networks, which specifically addresses the two problems raised above. In our approach, the network formation is simulated on a lattice with the help of a Monte Carlo procedure, which allows the formation of rings of any size. However, in contrast to the work of ref 4 and 5, the approach also takes into account the presence of entanglements latent in the polymer prior to cross-linking. That molecular network is continuously strained on the computer, and the following processes are allowed to occur: (i) extension and orientation of chain strands between junctions; (ii) slippage of chains through entanglements; (iii) breakage of strands at maximum elongation. At each value of the external strain, mechanical equilibrium is attained through a series of standard relaxation methods,[19] which steadily reduce the net residual force acting on each network junction.

Our model has been applied to elastomeric networks formed through end linking of difunctional polymer chains with plurifunctional junction sites. The dependence of mechanical properties on molecular weight of the starting polymer, cross-link functionality, and degree of advancement of the reaction has been studied.

2. Model

a. Network Formation. In our model, the elastomeric network prior to cross-linking is represented by an entangled network of (bifunctional) macromolecules, which are in a random coil configuration. That network is built on a computer, as follows. We start with a regular empty lattice of nodes, which represent potential elastically active junctions.[20] For simplicity, this paper will be restricted to the case of macromolecules having a molecular weight M larger than the molecular weight between entanglements, M_e. This implies that the distance between nodes be of the order of that between entanglements. These nodes are then connected with macromolecules having a prescribed molecular weight distribution (for details, see ref 21). In this paper, we deal solely with monodisperse molecular weight distributions for the starting polymer. Figure 1 depicts a small section of our network for a polymer having a molecular weight (M) equal to 4 times that between entanglements (M_e). Each macromolecule in Figure 1 is thus defined through a random walk connecting three nodes (entanglements) on the lattice. Details of the configuration of a molecular chain strand between two entanglements are omitted in the model, and only end-to-end vectors (wiggling lines) are being considered. Since the coordination number of an entanglement is only 4, the actual three-dimensional network has been given a planar (x–y) configuration. Periodic boundary conditions have also been imposed along the transverse x axis.

The nodes in Figure 1 are of three different types: nodes with four chain strands originating from them (type I); nodes with two strands (type II); nodes with 0 strands (type III). Nodes of type I represent true entanglements (denoted by a filled-in circle in Figure 2). Nodes of types II and III, on the other hand, are vacant, and the cross-linking procedure is initiated by filling them in with tetra- or trifunctional monomers (see Figure 2). These monomers react—with probability p—with the neighboring chain ends. Nodes of type II with two reacted chain ends lead to the formation of an additional entanglement (nodes type IV, see Figure 2); those with only one or zero reacted ends are not elastically active and are therefore removed from the lattice (node type V). Note that the local removal of nodes requires a careful updating of the number of statistical segments along neighboring chain strands. Similarly, nodes of type III with three or four reacted ends are considered as elastically active cross-links (nodes of type VI and VII), whereas the others are removed.

The procedure outlined above leads, for a given value of the molecular weight M and advancement of the reaction p, to the

0024-9297/89/2222-3633$01.50/0

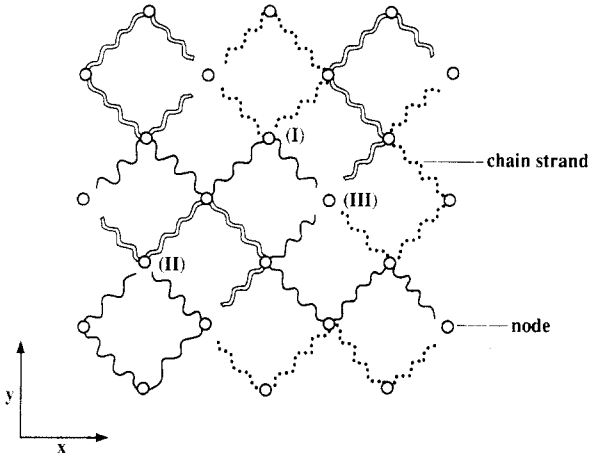

Figure 1. Schematic lattice representation of an entangled (x–y) network prior to cross-linking. The lattice nodes (O) are distributed on a regular lattice, and they represent potential elastically active junctions. The polymer has a monodisperse molecular weight (M) equal to 4 times that between entanglements (M_e). Details of the configuration of a molecular chain strand between two entanglements are omitted, and only end-to-end vectors (wiggling lines) are represented. Different line types are for different molecules. The lattice nodes are of three types: nodes with four chain strands originating from them (type I); nodes with two strands (type II); nodes with 0 strands (type III).

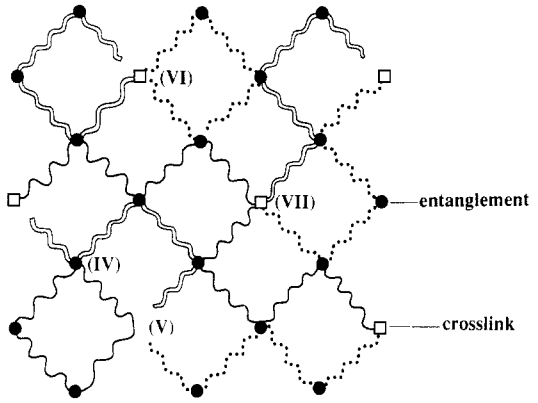

Figure 2. Same network as in Figure 1 but, after cross-linking with tetrafunctional monomers. Entanglements are designated by ●, whereas cross-links are denoted by □. For further details, see text.

formation of a network of junction points (entanglements and cross-links), all of which are elastically active. Among the active entanglements, however, only those trapped between cross-links are permanent. Since we are, in the present work, interested in measuring the effect of entanglements *at elastic equilibrium*, this leads to the need to further remove from the lattice all those entanglements, like node type IV in Figure 2, which are no independently connected to the network through four intact chain strands.

b. Deformation and Entanglement Slippage. The network, at this stage of the simulation procedure, is quite different from its initial representation in terms of a regular lattice of nodes. The removal of all elastically inactive nodes (described in section 2.a) has led to a very irregular structure whose deformation behavior is expected to be quite nonaffine. A correct description of the global stress–strain behavior thus requires knowledge of the local stress distribution around individual nodes. For a given value of the external stress, this is obtained through a detailed relaxation of every single junction point toward mechanical equilibrium with its connected neighbors. That relaxation is performed with the help of a series of computer algorithms, which steadily reduce the residual force acting on each junction (for details, see ref 21 and 22). The force f on a particular chain strand between two junctions is calculated by using the classical treatment of rubber elasticity[23]

$$f = (kT/l)\mathcal{L}^{-1}(\mathbf{r}/nl) - f_0 \qquad (2)$$

in which $\mathbf{r}$ and n denote, respectively, the length of the end-to-end vector and the number of statistical segments (of length l) for the strand. $\mathcal{L}^{-1}$ is the inverse Langevin function, whereas f_0 denotes the local force in the absence of strain, i.e., that for which $\mathbf{r} = n^{1/2}l$.[24]

The above relaxation procedure is very computer-time consuming since it requires a large number of iterations over the whole network before *all* the junction sites have reached mechanical equilibrium. Therefore, in order to save computer time, only displacements of the junctions along the tensile y axis are explicitly calculated. Assuming the structure to be incompressible, distances in the transverse x direction are contracted homogeneously by a factor $\lambda^{-1/2}$, where λ is the overall draw ratio along the y axis.[21] The elastically active junction points (cross-links and trapped entanglements) thus effectively more along parallel tracks in the y direction, which makes our study of the stress–strain dependence truly one-dimensional. The above simplification, without which the complexity of the computer code as well as the length of the calculations would be intractable, is justified because the axis of interest is the tensile y axis. It should also be of little importance in the present qualitative study of the effects of entanglements on deformation behavior.

The nonaffine displacements of the various junctions, obtained through network relaxation, create large force gradients on chains passing through trapped entanglements. These gradients lead to the possibility of chain slippage, which is allowed in the model until the difference in force in the two strands of a chain separated by an entanglement falls below the entanglement friction force. The latter, which is left as a free parameter, thus effectively prevents an entanglement from moving freely along the chain contour. Note also that the above treatment neglects the effects of chain–chain interactions along the length of the chain. The justification for that neglect is that friction at entanglement junctions essentially dominates the rheological behavior.

c. Model Parameters. The model described above has been applied to the end linking of difunctional polymer chains with plurifunctional monomers, in an attempt to describe the mechanical properties of poly(dimethylsiloxane) (PDMS) networks. According to Ferry,[25] the molecular weight between entanglements for that polymer, M_e, equals 8100 g/mol, which also corresponds to an average number of chain atoms $n' = 220$. Since the number of backbone atoms per statistical segment for PDMS is around 10,[26] a chain strand of $M = 8100$ contains $n = n'/10 = 22$ statistical segments. The precise numerical value for the statistical segment length l (see eq 2) is immaterial for our present purposes (see section 3). Typically, lattices of 60 × 60 nodes have been used in the calculations. The generation of a particular network and the testing of its mechanical properties take about 4 h of CPU time on an IBM 3090.

3. Results and Discussion

Figure 3 shows a typical network structure, as obtained from our computer model, prior to deformation. The starting molecular weight equals 4 times the molecular weight between entanglements, $M = 4M_e$, and the degree of advancement of the reaction $p = 0.96$. The functionality of the cross-linker is taken to be 4. The figure shows only the gel fraction with its elastically active junctions and their connecting strands. Dangling ends have not been represented. Elastically active cross-links (□) are connected to the network through at least three intact chain strands, whereas four strands are required for trapped entanglements (●). Note that chain strands, particularly near removed nodes, do not necessarily have the same number of statistical segments. A circle around an entanglement point denotes the presence of an internal loop. The network of Figure 3 is in local mechanical equilibrium; that is, for every strand $f = f_0$ (see eq 2 and ref 24).

The network properties for the case $M = M_e$ (no entanglements) are studied in Figure 4, as a function of the conversion factor p. The cross-linker is taken to be tetrafunctional. The figure shows results for the gel fraction

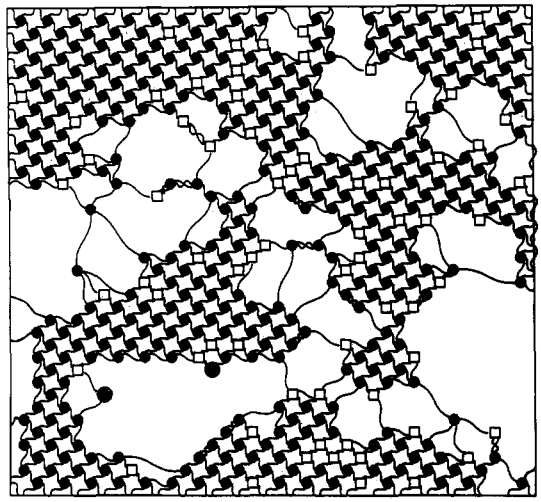

Figure 3. Actual network prior to deformation, as obtained from the computer model for a polymer with $M = 4M_e$ and cross-linked with tetrafunctional monomers. The fractional conversion of cross-linker groups is $p = 0.96$. The figure shows only the gel fraction with its elastically active junctions (cross-links, □; entanglements, ●) and their connecting strands. Dangling ends have not been represented. A circle around an entanglement point denotes the presence of an internal loop.

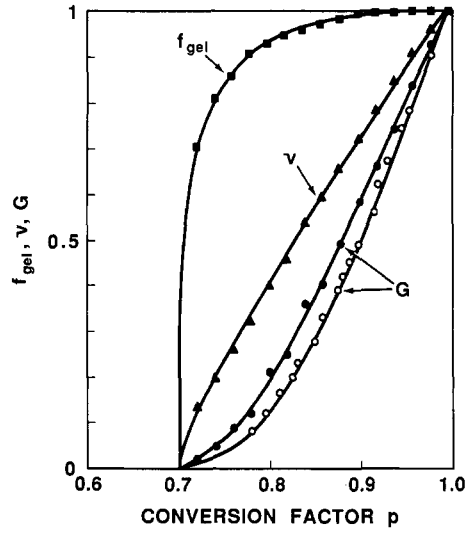

Figure 4. Network properties for the case $M = M_e$ (no entanglements) as a function of the conversion factor p. The cross-linker is taken to be tetrafunctional. The figure shows theoretical results for the gel fraction f_{gel} (■), density of elastically active chains ν (▲), and modulus G (●) as a fraction of their respective values for the case $p = 1$. The results are for a network of 60 × 60 nodes. Also represented are experimental data (○) reported by Valles and Macosko[27] for the modulus of tetrafunctional PDMS networks with $M_i = 11\,600$, a value close to that for M_e. The experimental value for p_c has been shifted to make it equal to the theoretical value.

f_{gel}, density of elastically active chains ν, and modulus G as a fraction of their respective values for the case $p = 1$. Our G values have been calculated from the overall stress in the small strain limit and under equilibrium conditions. The overall stress itself has been estimated from the axial force measured at one end of the network. The results are for a network of 60 × 60 nodes. The critical gel point for that finite system is around 0.69, which is close to the theoretical value $p_c = 0.5^{1/2} = 0.707$ expected for an infinite system. Our results show a low sensitivity of the gel fraction on the conversion factor for not too low values of p: at $p = 0.9$, the gel fraction is still 98.7%! The ν values, on the other hand, decrease almost linearly with p. These

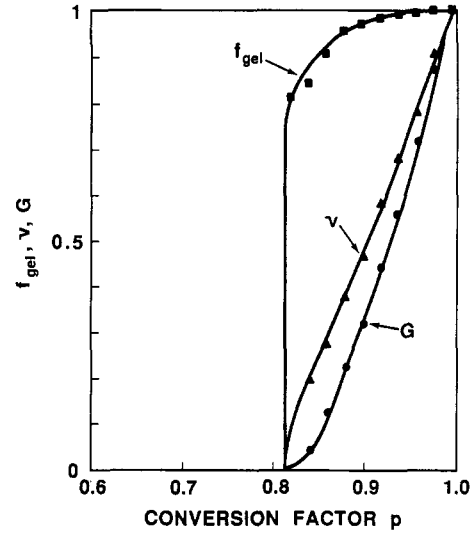

Figure 5. Same as Figure 4 but, for a trifunctional cross-linker.

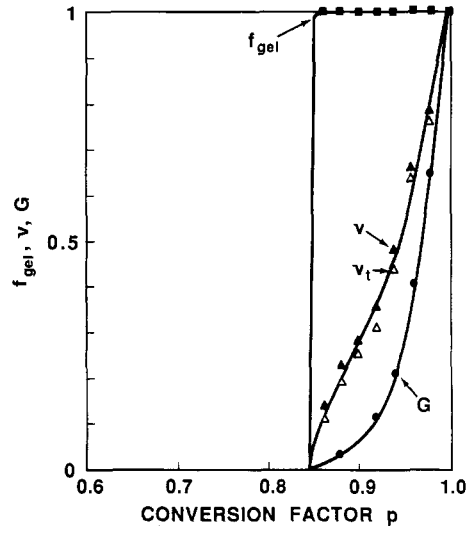

Figure 6. Network properties for the case $M = 4M_e$ (entanglements present) as a function of the conversion factor p. The cross-linker is taken to be tetrafunctional. The figure shows theoretical results for the gel fraction f_{gel} (■), density of elastically active chain strands ν (▲), trapped entanglements ν_t (△), and modulus G (●) as a fraction of their respective values for the case $p = 1$. The results are for a network of 60 × 60 nodes.

observations are quite similar to the analytical results of ref 14 based on Flory–Stockmayer classical theory. Even more important, however, is our finding in Figure 4 that the modulus G shows a faster decrease with p than that predicted from eq 1. This is due to the presence of elastically inactive internal loops, which are fully accounted for in the present approach. Also represented in Figure 4 are experimental data reported by Valles and Macosko[27] for the modulus of tetrafunctional PDMS networks, with $M_i = 11\,600$: a value close to that for M_e. A good agreement with our model calculations is found, although the experimental values seem to be systematically lower. This could be due to the fact that the latter are for a slightly entangled network ($M_i > M_e$), for which a sharper decrease of the modulus with p is expected (see Figure 6).

Our results for a trifunctional cross-linker (with $M = M_e$) are presented in Figure 5. The critical gel point is around 0.78, which is close to the expected value $p_c = (0.5 \times 4/3)^{1/2} = 0.816$. The results are qualitatively similar to those observed in Figure 4 for a tetrafunctional cross-linker.

The effect of molecular entanglements on network properties is studied in Figure 6. The figure is for a

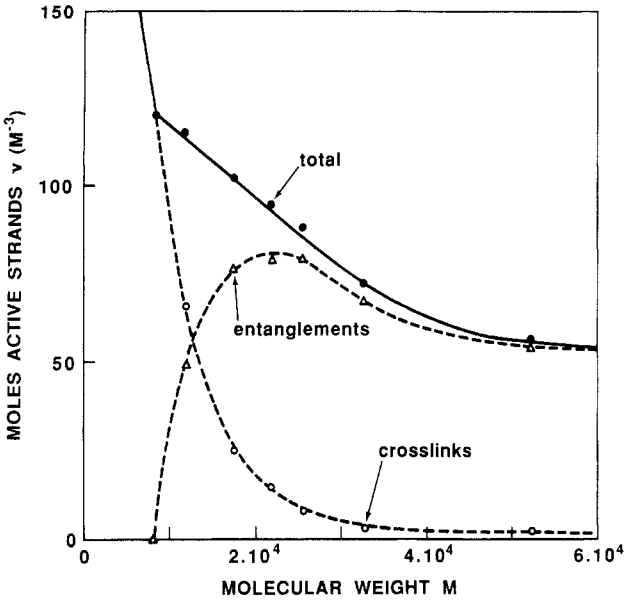

Figure 7. Dependence of the number of elastically active strands ν on the initial molecular weight for (close to) monodisperse PDMS (ρ = 1000 kg/m^3; M_e = 8100 g/mol). The results are for a tetrafunctional cross-linker with p = 0.98. The notation is as follows: ●, total number of active strands; △, contribution from trapped entanglements; ○, contribution from cross-links.

starting molecular weight $M = 4M_e$ cross-linked with tetrafunctional monomers. The first effect of the presence of entanglements is found in the gel fraction, which, at any $p > 0.85$, is much higher than that for the unentangled case (compare to Figure 4). Entanglements, however, also lead to much lower values of the density of elastically active strands ν. This is due to the presence in the gel of a large number of nonpermanent entanglements, which do not contribute to the elastic properties *at equilibrium*. The figure indeed also shows that the sharp drop in ν closely follows that of the density ν_t of permanent entanglements trapped between cross-links (△). Thus, even though their gel fractions are close to 100%, the networks in Figure 6 contain a number of quite long dangling ends, which have slipped through untrapped entanglements and do not contribute to the elastic properties. This is clearly exemplified by the modulus results G, which closely follow our ν_t (or ν) curves.

The relative contributions of cross-links and trapped entanglements to ν are studied in detail in Figure 7. The results are presented as a function of the starting molecular weight M for (close to) monodisperse PDMS. The figure is for a tetrafunctional cross-linker with p = 0.98. As a general result, the total number of elastically active strands decreases with the molecular weight and follows different regimes below and above M_e. A detailed analysis of the relative contributions of cross-links and entanglements gives the following insight. At low $M < M_e$ (=8100), entanglements are absent and all the active strands originate from cross-links. Within that regime, our results follow the expected relation $\nu \sim 1/M_e$. At $M > M_e$, entanglements trapped between cross-links start to play a contributing role to ν. Inspection of the figure shows that the latter contribution already exceeds that from cross-links at rather low values of M of the order of 2 to 3 times M_e. That finding is of the uttermost importance since those molecular weight values fall within the range of those usually reported for PDMS and many commercial rubbers. These results thus point to the relevance of the present approach, which takes full account of the effects of trapped entanglements on mechanical properties.

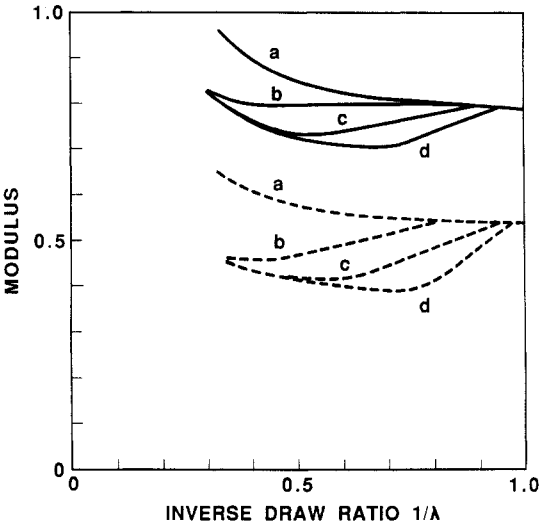

Figure 8. Dependence of the equilibrium modulus on the inverse draw ratio $1/\lambda$. The figure is for a tetrafunctional cross-linker and an initial molecular weight $M = 4M_e$. The two sets of curves are for different values of the conversion factor p: p = 0.99 (continuous curves) and p = 0.98 (dashed curves). Curves within each set correspond to varying entanglement friction forces f_e: f_e = 100 (curve a), f_e = 0.05 (curve b), f_e = 0.02 (curve c), and f_e = 0.01 (curve d). The modulus is in units of its limiting value for complete reaction p = 1 and under small strain conditions. In the absence of slippage (curve a), the networks break at $1/\lambda \approx 0.32$.

The model described above has been further applied to a detailed study of the effects of entanglements on the *equilibrium* stress–strain curves. To this end, the samples were stretched in small increments, and, at each extension, the stress was measured under mechanical equilibrium conditions. These conditions were considered to be met when (i) relaxation of the junctions with their neighbors was completed and (ii) no more slippage of chains through entanglements could be detected. Our results for the dependence of the equilibrium modulus on the (inverse) draw ratio λ are presented in Figure 8. The figure is for a tetrafunctional cross-linker and an initial molecular weight $M = 4M_e$. The two sets of curves correspond to different values of the conversion factor p: p = 0.99 (continuous lines) and p = 0.98 (dashed lines). Curves a–d within each set are for decreasing values of the entanglement friction force f_e. At high f_e = 100 (curves a), our computer results show no slippage of chains through entanglements, and the modulus increases with draw ratio, as expected from our use of the inverse Langevin function for the force (eq 2). At lower values of the entanglement friction force ($f_e < 0.05$, curves b–d), slippage sets in and this leads, at not too large λ, to a decrease in modulus with draw ratio. Inspection of the figure shows the decrease to be linear in $1/\lambda$, in perfect agreement with the empirical Mooney–Rivlin relation[28]

$$G = 2C_1 + 2C_2\lambda^{-1} \tag{3}$$

in which C_1 and C_2 are constants independent of strain. At higher values of λ, nonlinear effects in the Langevin function overcome that linear decrease and the modulus resumes its increase with draw ratio. Note that, in this regime, all the lines b–d converge toward a unique master curve. The latter, which runs parallel to curve a, describes the stress–strain behavior of the network in the limit f_e = 0.

The deformation behavior of the networks studied in Figure 8 (with p = 0.99) is illustrated in parts a–c of Figure 9. Figure 9a shows a typical configuration of the array of active cross-links (□) and trapped entanglements (●)

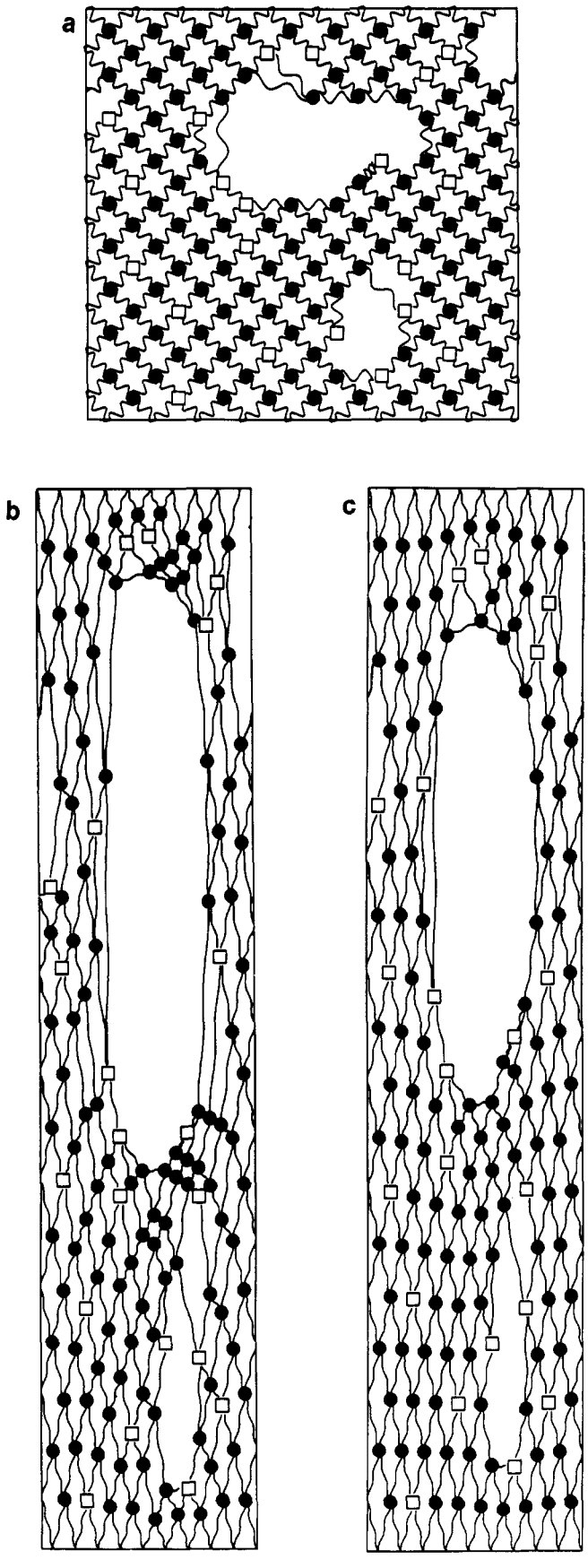

Figure 9. Networks of active cross-links (□) and trapped entanglements (●) for the samples studied in Figure 8 (with p = 0.99) at different stages of deformation: (a) network prior to deformation (λ = 1), (b) network at λ = 3 in the presence of entanglement slippage (f_e = 0.02), (c) same as in (b) but without slippage (f_e = 100).

for those networks prior to deformation (λ = 1). Again, dangling ends and elastically inactive junctions have not been represented for simplicity of the representation. This allows us to clearly identify in the figure the presence of two elastically inactive regions that act as network defects. Figure 9 show the deformation behavior of that structure at λ = 3, for different values of the friction factor f_e (f_e = 0.02, Figure 9b, and f_e = 100, Figure 9c). In the presence of chain slippage (Figure 9b), we observe an important increase in the distance between entanglements in the high-stress regions (left and right boundaries of the defects). This is accompanied by a densification of entanglement points in the low-stress regions (upper and lower boundaries of the defects). When slippage is absent (Figure 9c), the deformation behavior is seen to be more affine. As a result, the defect opening is much less pronounced than in Figure 9b.

In conclusion, we have presented a new model for the description of the factors controlling the mechanical properties of elastomers. The model is molecular in nature and explicitly takes into account the interactions between chains as well as the molecular weight distribution of the starting polymer. Our results definitely point to the importance of the role of entanglements on deformation behavior. These conclusions are in apparent conflict with those of previous studies by Mark and co-workers.[29,30] These authors indeed measured moduli values for PDMS, which satisfy eq 1 in its "chemical" limit, i.e., with ν calculated directly from the starting molecular weight value and assuming complete reaction. However, as correctly pointed out in ref 12 and 14, complete reaction is not physically attainable and the chemical contribution to ν could therefore be greatly overestimated. These conclusions are supported by our results of Figure 4. At p = 0.9, a gel fraction as high as 98.7%—a value in the range of those reported in ref 29 and 30—leads to a ν only 72% of theoretical. The figure also shows that, for those imperfect networks, the modulus exhibits a faster than linear decrease with the fraction of elastically active strands. Thus, it appears that chemical cross-links alone cannot fully describe the mechanical properties of cross-linked PDMS networks. This is particularly true since starting molecular weight values are commonly in the range 10 000 < M_n < 20 000, for which our results of Figure 7 predict an important effect of trapped entanglements.

References and Notes

(1) For an excellent review, see: Dusek, K.; MacKnight, W. J. In *Cross-Linked Polymers: Chemistry, Properties and Applications*; Dickie, R. A., Labana, S. S., Bauer, R. S., Eds.; ACS Symposium Series; American Chemical Society: Washington, DC, 1988; Chapter 1.
(2) Flory, P. J. *Principles of Polymer Chemistry*; Cornell University Press: Ithaca, New York, 1953.
(3) Stockmayer, W. H. *J. Chem. Phys.* **1943**, *11*, 45; **1944**, *12*, 125.
(4) Leung, Y. K.; Eichinger, B. E. *J. Chem. Phys.* **1984**, *80*, 3877; *Ibid.* **1984**, *80*, 3885.
(5) Galiatsatos, V.; Eichinger, B. E. *Rubber Chem. Technol.* **1988**, *61*, 205.
(6) Flory, P. J. *J. Chem. Phys.* **1977**, *66*, 5720.
(7) Ronca, G.; Allegra, G. *J. Chem. Phys.* **1975**, *63*, 4990.
(8) Flory, P. J.; Erman, B. *Macromolecules* **1982**, *15*, 800.
(9) Langley, N. R. *Macromolecules* **1968**, *1*, 348.
(10) Ferry, J. D. *Viscoelastic Properties of Polymers*, 2nd ed.; Wiley: New York, 1979.
(11) Dossin, L. M.; Graessley, W. W. *Macromolecules* **1979**, *12*, 123.
(12) Pearson, D. S.; Graessley, W. W. *Macromolecules* **1980**, *13*, 1001.
(13) Meyers, K. O.; Bye, M. L.; Merrill, E. W. *Macromolecules* **1980**, *13*, 1045.
(14) Gottlieb, M.; Macosko, C. W.; Benjamin, G. S.; Meyers, K. O.; Merrill, E. W. *Macromolecules* **1981**, *14*, 1039.
(15) Marucci, G. *Macromolecules* **1981**, *14*, 434.
(16) Gaylord, R. J. *Polym. Bull. (Berlin)* **1983**, *9*, 181.

(17) Ball, R. C.; Doi, M.; Edwards, S. F.; Warner, M. *Polymer* **1981**, *22*, 1010.
(18) Adolf, D. *Macromolecules* **1988**, *21*, 249.
(19) Allen, de G. D. M. *Relaxation Methods*; McGraw Hill: New York, 1954.
(20) A junction is elastically active if three or more of its arms are independently attached to the network.
(21) Termonia, Y.; Smith, P. *Macromolecules* **1987**, *20*, 835; *Ibid.* **1988**, *21*, 2184.
(22) Termonia, Y.; Meakin, P.; Smith, P. *Macromolecules* **1985**, *18*, 2246; *Ibid.* **1986**, *19*, 154.
(23) Treloar, L. R. G. *The Physics of Rubber Elasticity*, 2nd ed.; Clarendon: Oxford, 1958.
(24) The end-to-end vectors between nodes in the initial lattice are given a length $\mathbf{r} = n^{1/2}l$, with $n = 22$ (see section 2.c.). However, the removal of nodes after cross-linking leads to larger chain vector lengths $\mathbf{r}'$, which satisfy the relation $\mathbf{r}' = n'^{1/2}l$ only in the *average* sense. Chain vectors found not to satisfy that relation had their n' value readjusted. For conversion factors $p > 0.9$, this leads to a change in the average number of statistical segments per chain vector of no more than a few percent.
(25) Ferry, J. D. *Viscoelastic Properties of Polymers*, 3rd ed.; Wiley: New York, 1980; p 374.
(26) Van Der Hoff, B. M. E.; Buckler, E. J. *J. Macromol. Sci., Chem.* **1967**, *A1*(4), 747.
(27) Valles, E. M.; Macosko, C. W. *Macromolecules* **1979**, *12*, 673.
(28) Mooney, M. *J. Appl. Phys.* **1948**, *19*, 434; Rivlin, R. S. *Philos. Trans. R. Soc. London* **1948**, *A241*, 379.
(29) Mark, J. E.; Rahalkar, R. R.; Sullivan, J. L. *J. Chem. Phys.* **1979**, *70*, 1794.
(30) Llorente, M. A.; Mark, J. E. *J. Chem. Phys.* **1979**, *71*, 682.

Chain Dynamics, Mesh Size, and Diffusive Transport in Networks of Polymerized Actin. A Quasielastic Light Scattering and Microfluorescence Study

Christoph F. Schmidt, Michael Bärmann, Gerhard Isenberg, and Erich Sackmann*

Biophysics Group, Department of Physics, Technische Universität München, D-8046 Garching b. München, FRG. *Received December 8, 1988; Revised Manuscript Received February 13, 1989*

ABSTRACT: Dynamical (chain excitations, reptational diffusion) and structural (mesh size) properties of semidilute solutions (gels) of polymerized actin and their concentration dependencies were studied by quasielastic light scattering (QELS) and microfluorescence experiments. By QELS we could measure the internal dynamics of single chains. The fact that only internal single-chain dynamics are observed by QELS is a consequence of the inverse of the scattering vector $\mathbf{q}$ (6×10^4 cm$^{-1} \leq q \leq 3 \times 10^5$ cm^{-1}) being small compared to both the average contour length of the actin filaments (≥ 30 μm), which was estimated from reptational diffusion, and the average mesh size ξ of the network. That QELS measures internal dynamics of single chains is also shown by the insensitivity of the measured dynamic structure factor to cross-linking by α-actinin. For the range of actin concentrations, 0.08 mg/mL $\leq c_a \leq$ 0.37 mg/mL, and scattering angles, $20° \leq \theta \leq 150°$, studied in this work, the dynamic structure factor $S(\mathbf{q},t)$ of the polymer chains decays like $S(\mathbf{q},t) \propto \exp(-\Gamma_q^{(0)}t)$ at short times ($\Gamma_q^{(0)}t \ll 1$). At long times ($\Gamma_q^{(0)}t \gg 1$) it follows the relation $S(\mathbf{q},t) \propto \exp(-(\Gamma_a^{(0)}t)^{2/3})$. The initial decay rate $\Gamma_q^{(0)}$ exhibits a power law of the form $\Gamma_q^{(0)} \propto q^{2.76\pm0.1}$. Actin filaments thus approximate the universal behavior predicted for a Rouse–Zimm chain by Dubois-Violette and de Gennes (*Physics* **1967**, *3*, 181). The deviation from the predicted q^3 dependence of the initial decay rate is similar to that found for synthetic polymers by several groups. Concentration-dependent deviations from Rouse–Zimm behavior, which are most prominent for $\Gamma_q^{(0)}t \gg 1$, are attributed to filament interactions. Translational diffusion coefficients of fully polymerized actin filaments were measured by fluorescence photobleaching (FRAP). We obtained a diffusion coefficient of $D_{trans} \approx 8 \times 10^{-11}$ cm^2/s for $c_a = 1$ mg/mL. D_{trans} scaled roughly like $D_{trans} \propto c_a^{-1} \propto \xi^2$ as predicted by the reptation model for flexible chains. The average mesh size of actin networks as a function of actin concentration, c_a, was determined by measuring the translational diffusion coefficient, $D(c_a,d)$, of latex spheres of various diameters, d, by both FRAP and microscopic videotracking (Perrin technique). Scaling laws were applied to relate first $D(c_a,d)$ to the ratio d/ξ and second the mesh size ξ to the actin concentration c_a. $D(c_a,d)$ scales as $D(c_a,d) = D(0,d)\exp\{-\alpha[dc_a^{\nu}]^{\delta}\}$ with $\nu \approx 1/2$, $\delta \approx 2$, and $\alpha \approx 1$ as hypothesized by de Gennes et al. for a non-cross-linked network of rodlike polymers. The Rouse–Zimm-like behavior of actin filaments, as observed by QELS, contrasts with the appearance of actin as a semiflexible polymer in microscopic end-to-end distance measurements, which have been reported in the literature. This scale-dependent difference in apparent flexibility is suggested to be a consequence of the complex structure of actin filaments as a "polymer of polymers". We hypothesize that small-scale dynamics are dominated by stretching elasticity, i.e., by Rouse–Zimm-like excitations of filament subunits, whereas large-scale dynamics are determined by the bending elasticity of the filament. The crossover length between the two regimes would have to be of the order of micrometers. We point out the usefulness of actin gels as model systems to study fundamental properties of polymers on a mesoscopic scale with coil radii in the 100-μm regime. On this scale internal motions can be easily studied by quasielastic light scattering instead of neutron scattering.

Introduction

Actin filaments are a major component of the cell cytoskeleton. They are believed to play an essential role in cell motility, intracellular transport, and in the determination of the viscoelastic properties of cells.[1] A large number of actin binding proteins (some 20–30) have been identified which regulate the polymeric structure and the viscoelasticity of the actin network as well as its coupling to the cell membrane.[1] An actin filament can be viewed either as a one-start, left-handed helix with a 5.9-nm pitch or as a two-start, right-handed helix with a 71.5-nm pitch.[2] There is experimental evidence[3] that the longitudinal bonds are stronger than the lateral bonds, thus favoring

* To whom correspondence should be addressed.

0024-9297/89/2222-3638$01.50/0